



Solar Facilities for the European Research Area

SFERA-III

Solar Facilities for the European Research Area

Preliminary Results of the 3D-shape Round-Robin

Internal Deliverable

Estimated delivery date: N/A

Actual delivery date: 31.01.2024

Lead beneficiary: ENEA

Person responsible: Marco Montecchi

Deliverable type: R DEM DEC OTHER ETHICS ORDP

Dissemination level: PU CO EU-RES EU-CON EU-SEC



THIS PROJECT HAS RECEIVED FUNDING FROM THE EUROPEAN UNION'S HORIZON 2020 RESEARCH AND INNOVATION PROGRAMME UNDER GRANT AGREEMENT NO 823802

AUTHORS

Author	Institution	E-mail
Marco Montecchi	ENEA	marco.montecchi@enea.it
Arcangelo Benedetti	ENEA	arcangelo.benedetti@enea.it
Giuseppe Cara	ENEA	giuseppe.cara@enea.it
Francisco Torres	FISE	francisco.torres@ise.fraunhofer.de
Gregor Bern	FISE	Gregor.Bern@ise.fraunhofer.de
Marc Röger	DLR	Marc.Roeger@dlr.de
Eckhard Lüpfert	DLR	Eckhard.Luepfert@dlr.de
Devon Kesseli	NREL	Devon.Kesseli@nrel.gov
Guangdong Zhu	NREL	Guangdong.Zhu@nrel.gov
Braden Smith	SANDIA	bsmith4@sandia.gov
Randy Brost	SANDIA	rcbrost@sandia.gov

DOCUMENT HISTORY

Version	Date	Change
1	22.12.2023	
2	08.01.2024	With DLR and SANDIA results
3	06.02.2024	With DLR, NREL and SANDIA set-up description and some NREL results
4	19.02.2024	Text modified according to the participants' indications Data analysis improved and extended

VALIDATION

Reviewers	Validation date
Marc Röger	20.02.2024

DISTRIBUTION LIST

Date	Recipients
24.02.2024	Participants of the round robin test

Disclaimer

The content of this publication reflects only the author's view and not necessary those of the European Commission. Furthermore, the Commission is not responsible for any use that may be made of the information this publication contains.

Executive Summary

In the framework of SFERA-III WP10 Task3, ENEA has organized the 3D-shape round-robin (RR); the purpose is to compare the main geometrical parameters of 3D shape measurement of parabolic-trough (PT) reflective panels evaluated with the instruments adopted by each participant among:

- ENEA
- DLR
- F-ISE
- NREL
- SANDIA

The last two institutions are outside of the EU, but benefited from the *Transnational Access* institute to visit several European laboratories, including the ENEA Casaccia research center where they accomplished some measurements with a portable experimental set-up.

RR is based on the inter-laboratory circulation of 3 inner plus 3 outer PT panels.

The start of the RR was delayed by the covid pandemic, then the circulation of the specimen-set and their measurement took more than one year. At the time of drafting this deliverable at the end of SFERA-III project, NREL has not yet completed the analysis of the measurements, making available only the deviations of the slopes. Therefore here will be reported only the preliminary results. The full comparison will be published as soon as possible, maybe in the open access venue Open Research Europe.

Table of Contents

Executive Summary	44
Table of Contents	5
1. INTRODUCTION	6
2. MEASUREMENT EQUIPMENT	7
2.1 ENEA – VISproPT	7
2.2 F-ISE	10
2.3 DLR	13
2.4 SANDIA – SOFAST	16
2.5 NREL	19
3. THE RRcomparator SOFTWARE	22
4. 3D SHAPE COMPARISON	24
4.1 Acceptance checkpoint	24
4.2 Comparison with the mean surface	28
5 COMPARISON of the deviations from the ideal parabola.....	36
6 CONCLUSIONS	47
6 REFERENCES	48

1. Introduction

In the framework of WP10 Task 3, ENEA enriched its Optical Laboratory with the new optical profilometer VISproPT, devoted to the 3D-shape measurement of parabolic-trough (PT) reflective panels. Due to the Covid pandemic, the new instrument has become fully operational only since September 2022. A detailed description of the VISproPT is given in [1], while the related software is today offered as open source at [2].

In order to exploit the original approach used in the VISproPT, ENEA organized a new round-robin (RR) on 3D shape measurements of panels for PT solar collectors; a previous attempt, accomplished about 10 year ago in the SolarPACES TaskIII framework [3], did not give satisfactory results because the differences among the results obtained by the participants were greater than the experimental error; as a matter of fact, today a dedicated guideline on the topic is still missing.

The proposal was accepted by F-ISE and DLR and then was extended to the National Renewable Energy Laboratory (NREL) and Sandia National Laboratories (SANDIA), which benefit from the Transnational Access tools offered by SFERA-III to send teams to Europe for visiting research infrastructures and participating in the introductory meeting to the round robin itself.

ENEA studied a method to ensure the reproducible placing of the PT panels in any laboratory; a document [4] describing in detail the procedure to be used was distributed to the participants in July 2022.

The box containing 3 inner and 3 outer panels for solar collector type LS3 (focal length 1710 mm), as well as the mechanical parts to make the supporting system, was shipped from ENEA to F-ISE in January 2023. After the measurements, in April 2023 F-ISE shipped the box to DLR, which completed the measurements and shipped the box to SANDIA in July 2023. Today NREL has not yet completed the data processing, thus only part of the required data are available and included in this report.

2. Measurement equipment

This section offers a short overview of the experimental equipment used by the RR participants.

2.1. ENEA - VISproPT

A detailed description of the VISproPT is given in [1], while the related software is offered as open source at [2].

In short, the VIS method [5] just needs of a good monochrome digital camera and a structured light source; the source type and the arrangement of these components around the object to be measured depend on the specific case.

The engineered version of the VISprofile is named VISproPT to distinguish it from the other instrument, named VISproLF [6], designed for 3D shape measurements of panels for linear Fresnel collectors.

The optical sketch adopted in VISproPT is shown in Figure 2.1-1, while the hardware, manufactured by MARPOSS Italia Spa [7], is shown in Figure 2.1-2. The PT panel to be investigated is placed on 4 supports (1,2,3,4) aligned on the same horizontal plane and positioned accordingly to the panel design.

Initially, the origin of the laboratory reference frame (LabRF) was approximately set in the centre of the 4 attaching points, with the Z axis aligned along the vertical and the X axis parallel to the motorized rail (and the direction of curvature of the panel). On the other hand, for the sake of comparison, in the RR the origin of LabRF must be placed in an unequivocally defined point like the centre of the metallic ball at the attaching point P2, which is the master one; the other attaching points are slaves (see [4]). The transformation of the coordinate system is very easy.

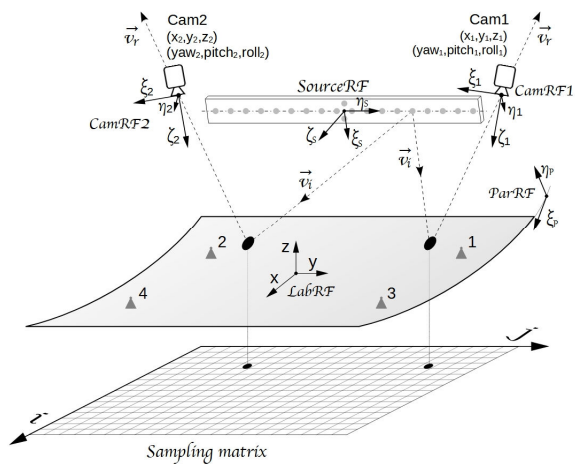


Figure 2.1-1. VISproPT optical sketch: two digital cameras (Cam1 and Cam2) acquire photos of the panel surface with the reflected images of the point source array. Five reference frames (RF) are used in the image-processing: 1) parabola (ParRF), 2) laboratory (LabRF), 3) point source array (SourceRF), 4) Cam1 (CamRF1), 5) Cam2 (CamRF2). At the end of the image processing, the experimental values of height and partial derivatives of the surface are gridded over the sampling matrix.



Figure 1.1-2. VISproPT hardware. The main components are: the point source array, two digital cameras and the motorized rail for moving the cameras over the specimen.

2.2. F-ISE

The local surface slope deviations of the parabolic-trough (PT) reflective panels of the 3D-shape round-robin were measured with the Fringe Reflection Technique (FRT) at Fraunhofer ISE laboratory. FRT is a deflectometry-based measurement method, which in principle, a camera directed at the mirror surface, in this case the parabolic trough mirror, records a distorted reflection of a sinusoidal pattern displayed by a projector, as shown in Fig. 2.2-1. In the laboratory setup, the camera is placed on the ceiling of the laboratory, the parabolic mirror on the ground, while the projector on the ground displays the sinusoidal pattern on the ceiling.

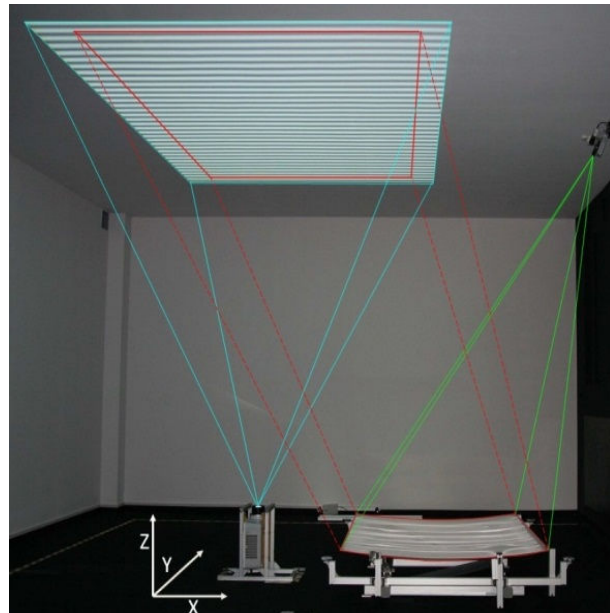


Figure 2.2-1. Deflectometry setup at Fraunhofer ISE for the shape measurement of the parabolic trough mirrors. On the top right, the camera is fixed, so the distorted reflection of the sinusoidal pattern can be recorded. On the bottom is placed the parabolic trough mirror and next to it the projector, which displays the sinusoidal pattern on the ceiling of the laboratory. The red square on the pattern is the area which the camera can record.

The LCD projector has a XGA (1024 x 768) resolution with a pixel width and height of 0,27 mm. The camera has a focal length of 12 mm, resolution of 1936 (H) x 1458 (V) and a pixel width and height of 3,69 µm.

A software algorithm evaluates the pattern and calculates the surface normal for each point imaged in a camera pixel, see 2.2-2. The advantage of the method is a spatially resolved measurement of the entire reflector area seen by the camera with a fine lateral resolution and information on the shape, surface gradients and microstructure.

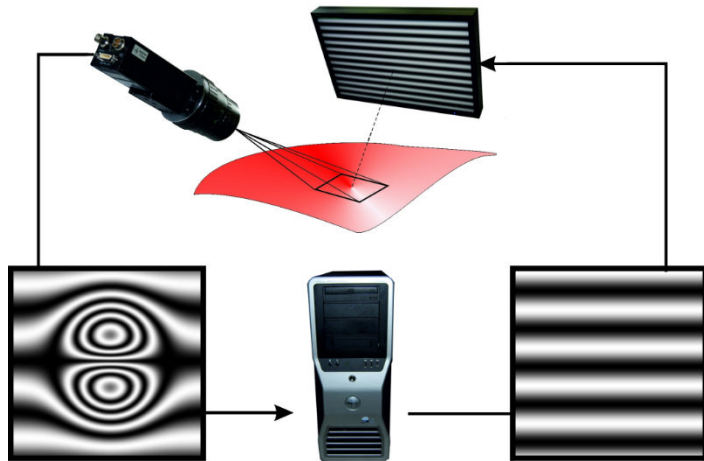


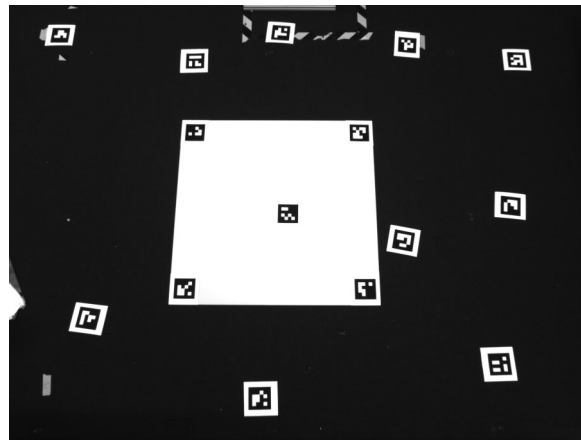
Figure 2.2-2. Sketch of the measurement process. A camera records multiple reflected patterns according to a phase-shifting technique. Shape irregularities on the specular surface result in distorted fringe patterns, which are evaluated to determine the actual surface slope. In the setup at Fraunhofer ISE, the screen which projects the pattern is replaced by a projector.

The calibration of the system is carried out using a laser scanner which extracts the world coordinates of squared markers placed on the ground and displayed on the ceiling from the projector (2.2-3A). Similarly, the camera takes a picture of the markers on the ground, obtaining the pixel coordinates of the markers (2.2-3B). Finally, an algorithm correlates the world coordinates of the laser scanner with the pixels of the camera for each marker.

The reference system is typically chosen as the centre of the laser scanner, which in frame of this projects, is changed to the centre of one of the metallic balls of the measurement setup defined in the document “Procedure for placing PT-panels in SFERA-III WP10 Task3 3D shape measurement round robin”[4].



A



B

Figure 2.2-3. A) Image taken from the laser scanner, which provides the world coordinates in X,Y,Z of the displayed markers on the ground and on the ceiling. The plane XY is defined conveniently parallel to the ground of the laboratory and Z normal to the plane. **B)** Image taken from the camera to the markers on the ground. This picture contains the information of the pixels of the markers which is later correlated to their X, Y and Z world coordinates.

2.3. DLR

Deflectometry is a method for measuring the slope of a reflective surface with high accuracy and spatial resolution and has been developed in the recent years in DLR and other research centers. In the DLR setup, a pattern which is projected onto a target and which is reflected by the surface of the mirror is used. From the reflection observed in the mirror with a CCD camera, the spatial coordinates of the CCD, the reflection on the mirror and the point of origin on the target can be assigned to each other. From this, the normal vector of the mirror at this point can be determined. In general, several images of fringe patterns with sinusoidal brightness distribution and different frequency and phase are necessary to achieve the assignment of the location coordinates clearly and with the desired accuracy, see Fig. 2.3-1

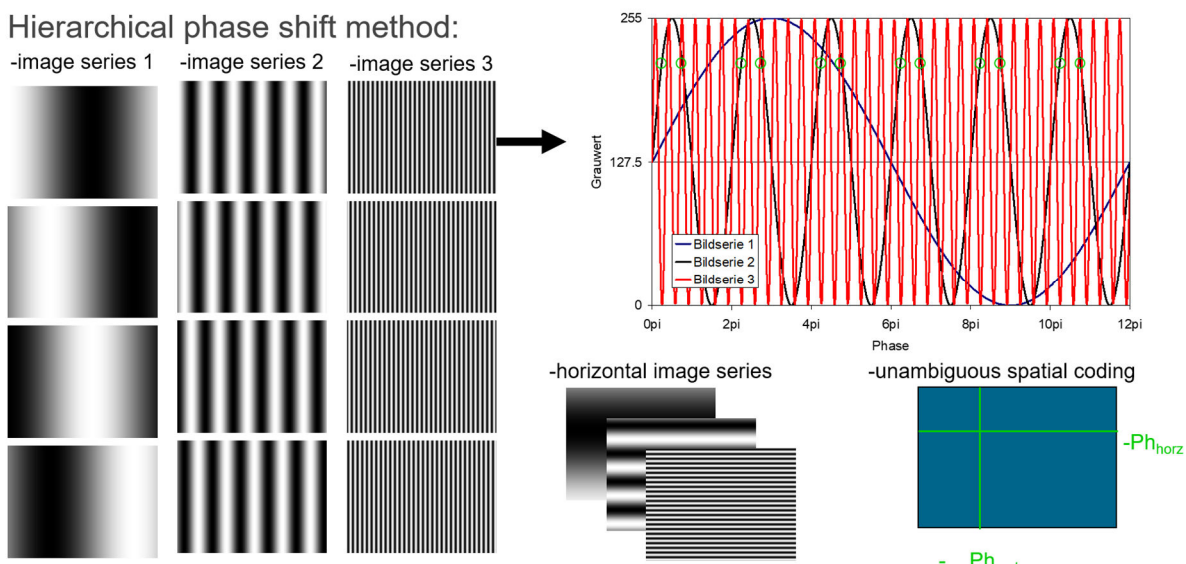


Figure 2.3-1. Hierarchical phase shift method used in DLR deflectometry.

This measurement technique has been successfully applied to dishes, heliostats, parabolic troughs and individual mirror components, see e.g. [8-12].

The measurement setup requires at least two permanently installed cameras and a target for projecting the fringe patterns. The space required depends on the mirror size and curvature as well as the number of measuring cameras used. If space is limited, the measurement object can be recorded with several cameras and overlapping image sections. During the measurement, which takes a few minutes,

the measuring room must be darkened. With a permanently installed setup, the preparation is limited to the exact positioning of the concentrator.

The measurement accuracy of deflectometry depends on the measurement configuration. In general, large distances between the target, mirror and camera have a positive influence on the measurement accuracy. In the case of parabolic-trough (PT) reflective panels in industrial fabrication lines or research laboratories, space is limited. The deflectometry setup in the DLR QUARZ laboratory is shown in Fig. 2.3-2.

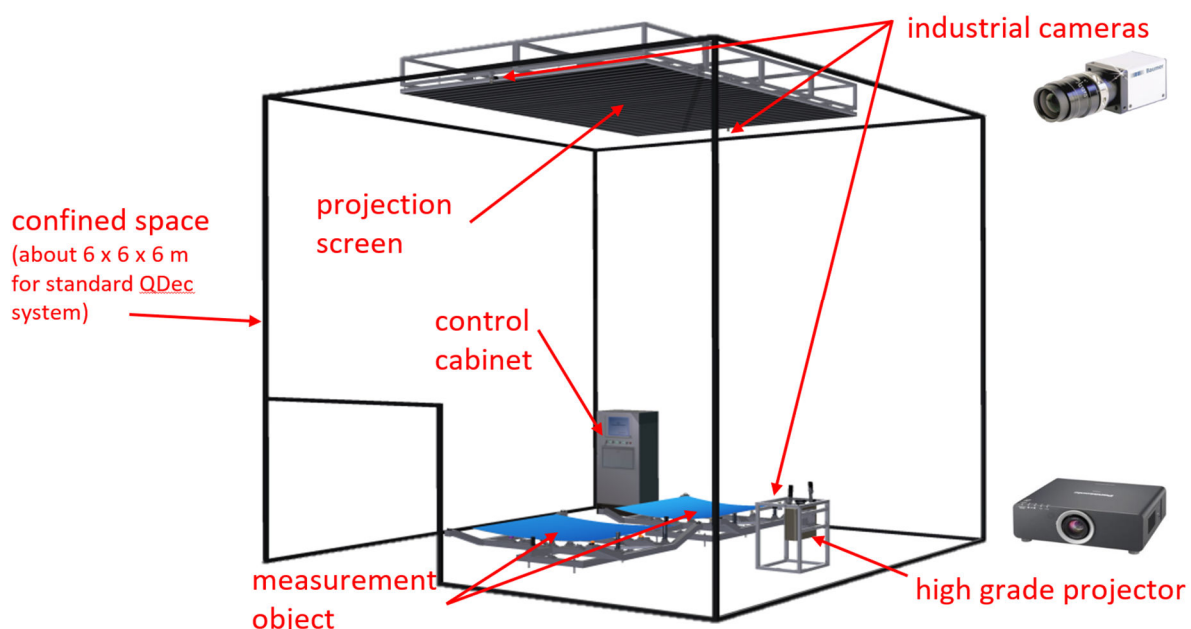


Figure 2.3-2. DLR deflectometry setup “QDec”

The measurement accuracy of the DLR setup is very good. To check measurement repeatability the same module was measured over the period of a day to see influence of temperature ($\Delta 5.5^{\circ}\text{K}$) especially on structure expansion. Twelve independent measurements were compared for local differences and very low standard and mean values below 0.05 mrad (1 sigma) indicate high repeatability.

The combination of dust loads and external lighting conditions can lead to failures in stripe detection and evaluation. However, high dust loads (just 30% reflectivity) are acceptable if a dark room is used. With constant ambient light, medium dust load (50 % reflectance) is acceptable. Dynamic light reflexes on mirror and screen have to be avoided during picture taking.

The measurement uncertainty was validated using a reference water surface, which is perfectly flat, see Fig. 2.3-3.

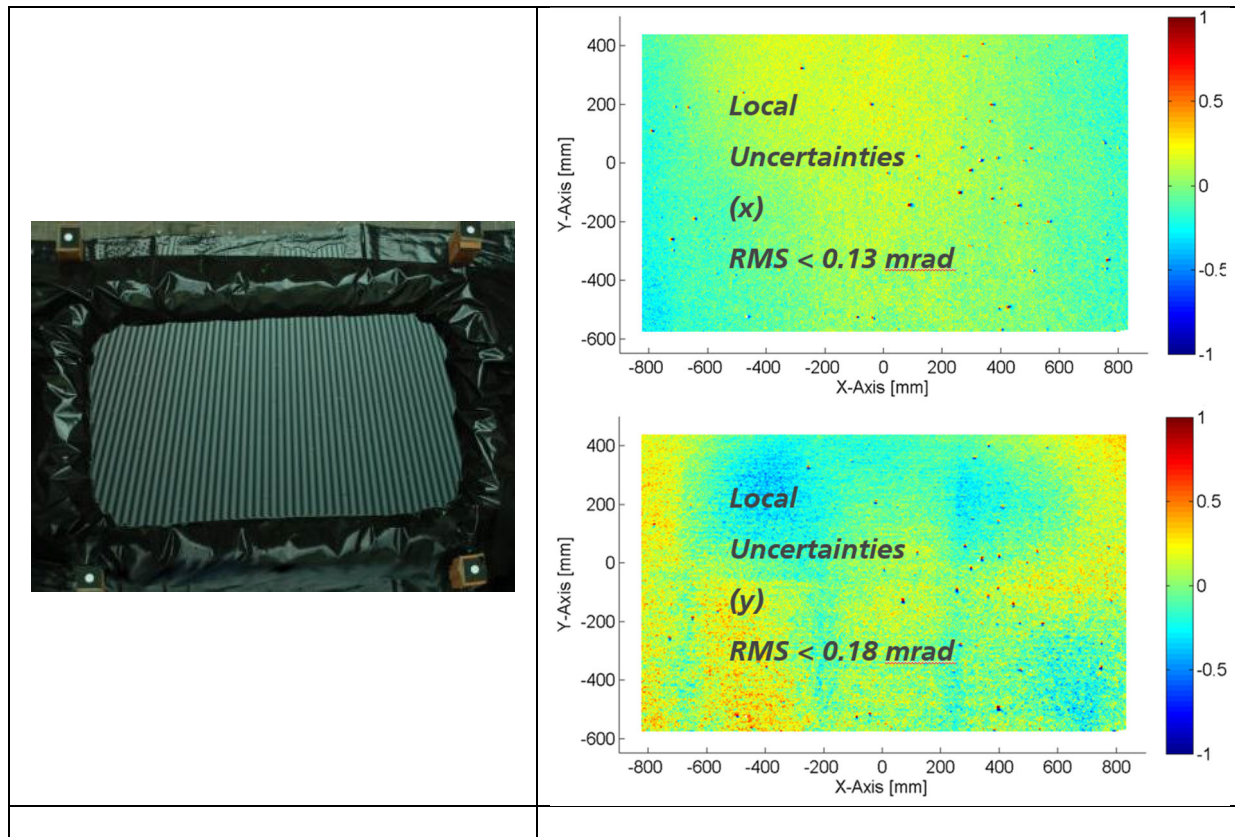


Figure 2-3-3. Validation of deflectometry with water reference surface

The achieved deviation between measurement and reference water surface was below 0.2 mrad (RMS value) and local uncertainties below 0.18 mrad. This is well below the expected and guaranteed local uncertainties, which is shown in Tab 2.3-1:

Tab 2.3-1. RMS and local uncertainties of DLR / CSP Services QDec system

Quantity	Uncertainty value
Panel uncertainty RMS	±0.2 mrad (1 sigma)
Local uncertainty	±0.5 mrad (1 sigma)

The deflectometry system, initially developed by DLR, has implemented in test laboratories and production lines by the DLR spin-off CSP Services (<https://www.cspservices.de/quality-control/>)

2.4. SANDIA - SOFAST

Sandia National Laboratories measured the surface slope of the SFERA mirrors with the deflectometry tool, SOFAST (Sandia Optical Fringe Analysis Slope Tool) [13, 14]. This software is now written in Python and will soon be available open source. If interested, contact OpenCSP@sandia.gov for further information.

The physical layout of a SOFAST setup consists of a camera, projector, and a screen. The specific layout used for the SFERA measurements is shown in Figure 2.4-1.

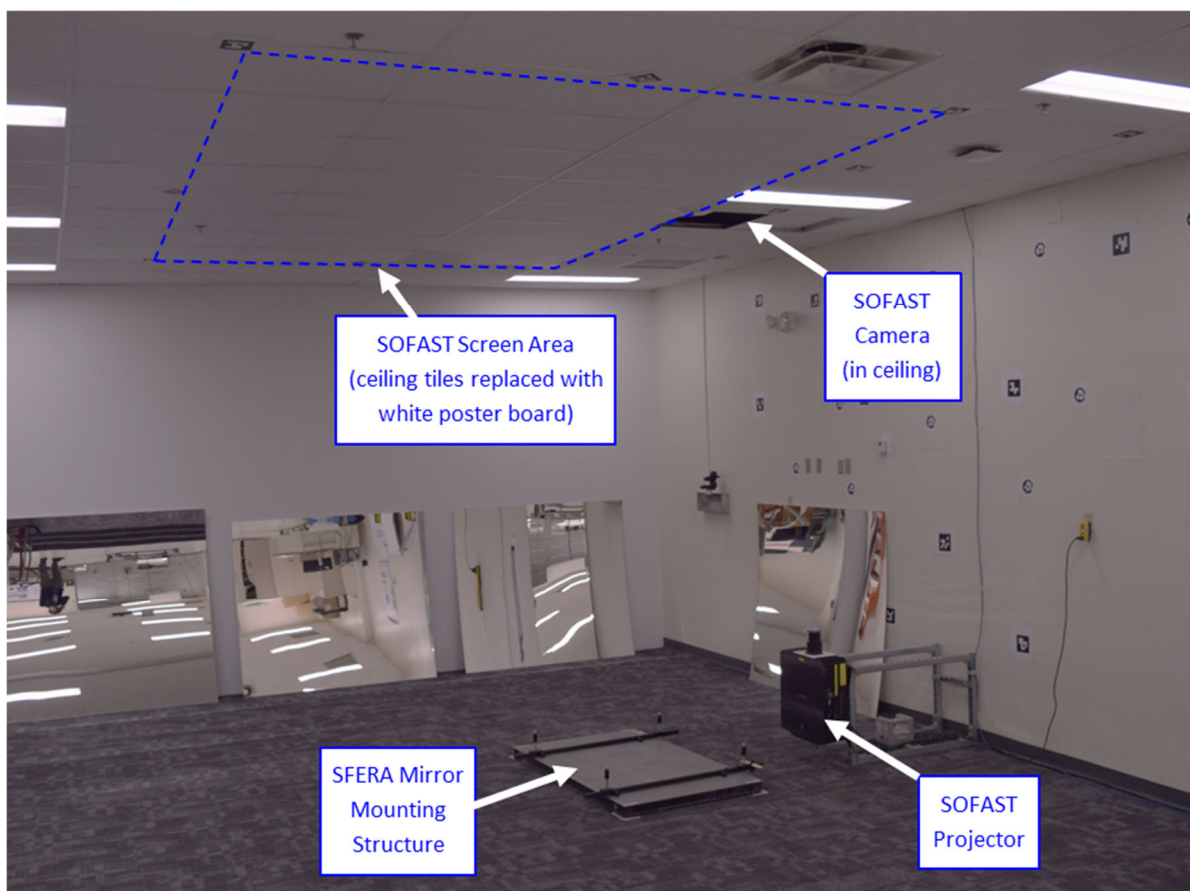


Figure 2.4-1. Layout of SOFAST measurement setup. The camera fixed in the ceiling views the reflection of sinusoidal fringes projected on the screen on the ceiling. The mirror mounting structure on the floor holds the four metallic balls used to support the SFERA-III mirrors.

During operation, regular sinusoidal fringe patterns are projected on the screen on the ceiling. The camera views the reflected sinusoidal fringes seen in the mirror. Distortions of the straight fringe patterns are interpreted by a processing algorithm as surface slope variations of the mirror. Over the course of a SOFAST measurement, the fringe periods transition from coarse to fine in both x and y directions; each finer fringe set increases the resolution of the measured surface slope. Figure 2.4-2

illustrates the four fringe periods used in the x direction.

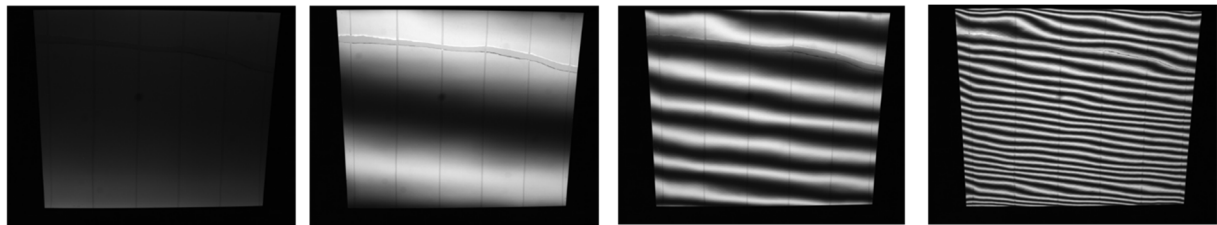


Figure 2.4-2. Example images as seen by the SOFAST camera of the x-direction fringes reflected in a SFERA mirror.

The SOFAST system is calibrated using photogrammetry. Photogrammetric targets called Aruco markers (some are visible on the back wall in Figure 2.4-1) are placed around the SOFAST screen, on the walls, and on the floor in the view of the SOFAST camera. As illustrated in Figure 2.4-3, a calibrated camera takes many pictures of the markers, and an algorithm calculates the position of the markers in space. The markers in the field of view of the SOFAST camera locate the camera relative to the screen.

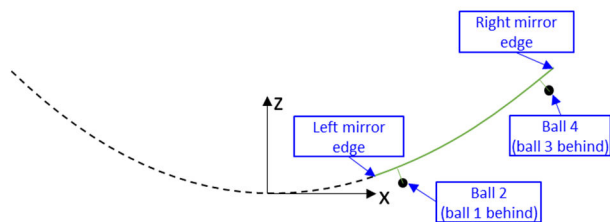


Figure 2.4-3. Example images from the photogrammetric SOFAST calibration procedure. Images of the scene (left) are used to calculate the relative positions of each marker. Located markers in the SOFAST camera's field of view (right) locate the camera relative to the screen.

SOFAST measures the mirrors and data is initially provided in the reference frame of the coordinate system that defines the parabolic surface of the mirror. We then transform the data into the “lab reference frame” as described in the SFERA procedure document. This transformation is illustrated in Figure 2.4-4.

Note that SOFAST is designed to be a slope measurement system; surface position estimates are provided for this comparison, but are not the program’s focus.

Data in SOFAST reference frame



Data in lab reference frame

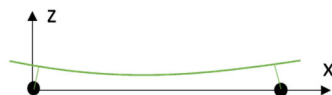


Figure 2.4-4. An illustration of the transformation of the surface slope data from the initial SOFAST reference frame (defined by the parabolic surface) into the “lab reference frame,” centered about metal ball number 2.

We measured a water pool as a ground truth reference. The water pool size was 2025 mm × 1320 mm. A still water pool will follow the curvature of the Earth; for a pool of this size, the resulting slightly convex surface will have a change of slope of approximately 0.00038 mrad across its diagonal. Since this is much lower than the target tolerances of this test, we will view the water pool as perfectly flat.

Figure 2.4-5 shows the measurement result. After executing an automated refinement of the calibration parameters, and excluding meniscus areas near pool edges or floating pieces of lint, the resulting slope map had an RMS error of 0.08 mrad. Further, peak-to-valley variation was less than 0.15 mrad over most of the surface. However, some higher slope deviations are seen in the lower right corner; we are still investigating these.

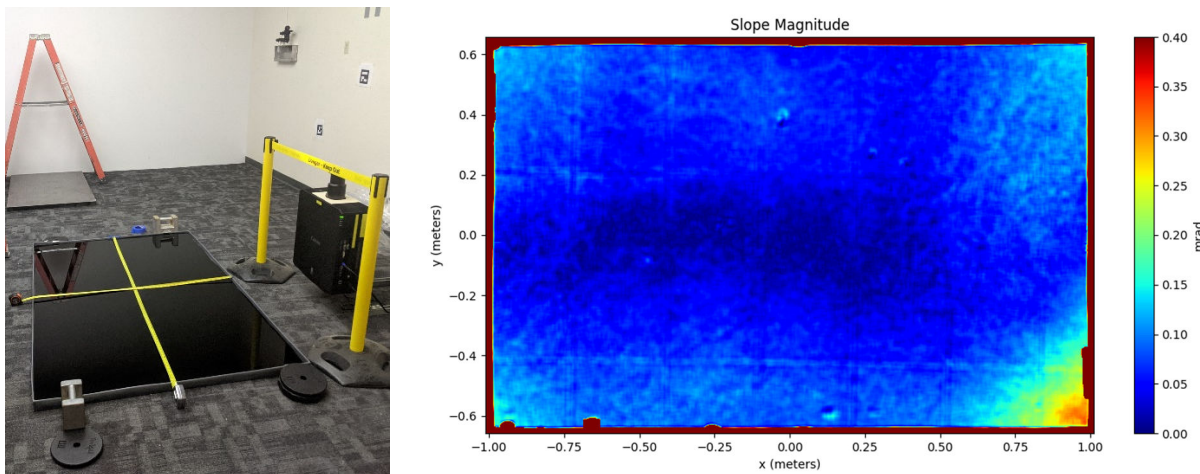


Figure 2.4-5. Testing the SOFAST measurement setup with a reference water pool.

2.5. NREL

The US National Renewable Energy Laboratory (NREL) participated in the round robin study using a lightweight optical measurement system called the Reflected Target Non-intrusive Assessment (ReTNA). This system calculates optical surface shape error by measuring the deflection of a printed coded target pattern. One main benefit of this system is that it is small and portable. All necessary equipment to collect a measurement, excluding the mirror and the mirror mounting platform, was brought to ENEA and Sandia in a suitcase to collect NREL's measurements on the round robin mirrors.

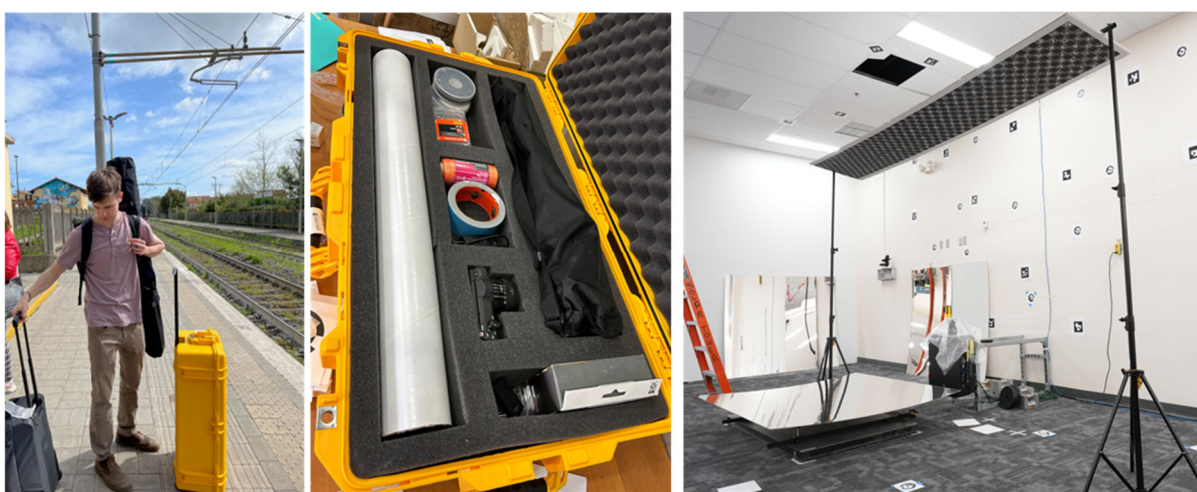


Figure 2.5-1: Left and center: the ReTNA equipment, consisting of a target stand (black bag), a rolled up adhesive target, and camera equipment (yellow case). Right: The ReTNA measurement setup at Sandia.

To collect an optical measurement, OpenCV computer vision tools are used to identify each coded ArUco target in a series of calibration images. Each coded target position is solved in space using photogrammetry, reducing the need for a flat target or precise positioning of the target panel. After the target is located in space, a series of images are collected of the target's reflection moving across the mirror. The same computer vision tools are used to identify the reflected target markers in these images. Deflection measurements from each image are combined into a surface map of the full mirror, and then interpolated onto a regular grid, as shown in Figure 2.5-2.

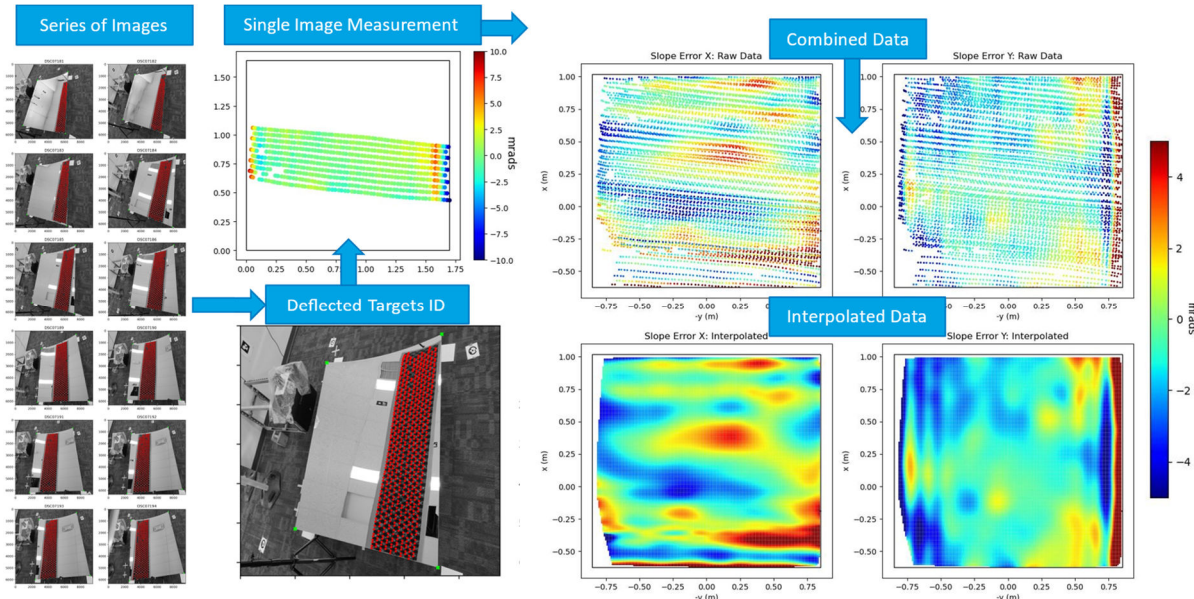
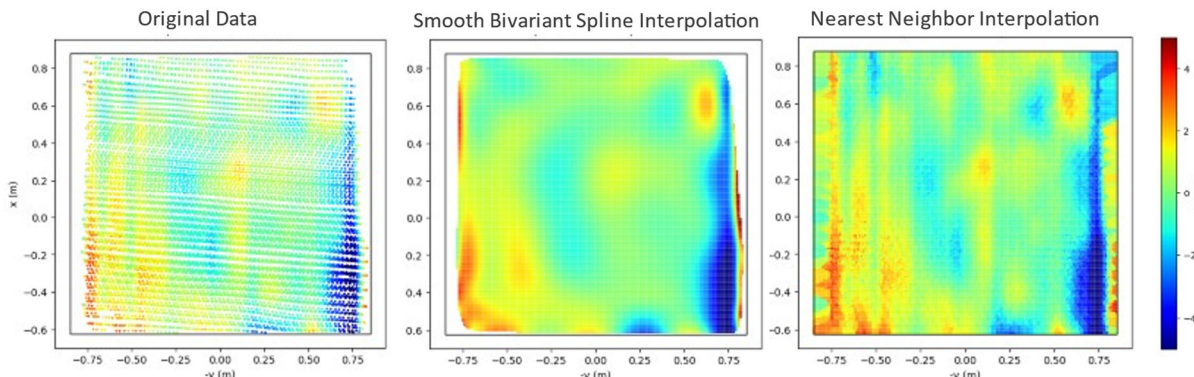


Figure 2.5-2: Basic ReTNA workflow. Results shown on the right are for round robin mirror id #60.

There are still some limitations in the portable system that NREL is working to resolve. One limitation in the physical setup was the length and rigidity of the portable target stand taken to Sandia, which prevented the reflection from spanning the entire mirror. This is evident in the unresolved left edges in Figure 2.5-2. In the future, this can be corrected with a larger target stand. A reflected target system also will have lower measurement resolution compared to a fringe deflectometry system. NREL researchers think that using a larger number of images can help systems like ReTNA achieve resolutions needed for most optical measurement applications. Lastly, several different methods can be used to interpolate unstructured measurements onto a regular grid. This is particularly important for highly unstructured results that ReTNA generates and can have an effect on the rms results. Two methods are shown in Figure 2.5-3.



Finally, NREL would like to acknowledge that our testing at ENEA and Sandia was supported by researchers at these institutions, without whom our participation would not have been possible.

3. The *RRcomparator* software

To make the comparison replicable to everyone, ENEA wrote in C++ the dedicated software *RRcomparator*, downloadable as open source from [15] together with the MS Windows executable, and the full set of experimental results provided by each participant.

The Graphical User Interface(GUI) and few examples of plots and 2D contour maps generated by the software are shown in Fig. 3.1. Please note that the scale of the contour-maps is the one used in the paired plot of the profiles for the two sections P2-P4 (green) and P1-P3 (red).

For a given specimen, to be loaded in RRcomparator, the results obtained from each evaluator must be arranged as a text file composed by row containing the values

x y z slopeX slopeYdevZ devSlopeX devSlopeY

where x,y are the coordinate (mm) in the Laboratory reference frame of a point of the reflecting surface having height z and the partial derivatives slopeX and slopeY; the remaining values are the *deviation* from the ideal parabola. The origin of the Laboratory frame is in the centre of the metallic ball of the master supporting pedestal P2 (see [4]).

In order to allow the point by point comparison, the results when loaded in *RRcomparator* are re-samples across a regular 2D-grid, with step 10 mm, placed in the plane XY.

Once specimen and feature (z, slopeX, slopeY, devZ, devSlopeX and devSlopeY) are set, the statistical analysis of the results obtained by a given participant as well as that of the difference (point by point) between a couple of participants or one participant and the Mean surface or the Ideal parabolic shape can be computed; the main results such as mean value, RMS, Peak-Valley, minValue and maxValue, are displayed in the “Tab statistics” and in the bottom of the GUI, for individual and comparison analysis, respectively.

From version 3.0, optionally the experimental surface can be “realigned” in order to set to 0 the difference on the attaching points with respect to the z value expected for the ideal parabola or the experimental devZ values; further details will be given in the

next section.



Figure 3-1. Graphical User Interface and examples of plots and 2D contour maps generated by the RRcomparator software.

4. 3D shape comparison

4.1. Acceptance check-point

The RR is based on the inter-laboratory circulation of 3 inner plus 3 outer PT panels designed for collector type LS3 with focal length 1710 mm. Each panel is hung on the supporting structure by means of four ceramic pads with a threaded metal nut inserted; these pads are glued on the back side in well defined positions.

Independently from the manufacturing technology, any reflecting panel is not completely rigid, therefore the 3D shape of its surface depends on how the sample is supported. On the other hand, for the sake of the success of RR, only the good reproducibility of the panel-placing is important, even if obtained by unusual manner, not representative of the normal usage.

As described in detail in [4] and shown in Fig 4.1-1, four identical metallic balls are screwed in the ceramic pads; four post-holders are arranged in the Lab so that the ball centres lie on the same horizontal plane.

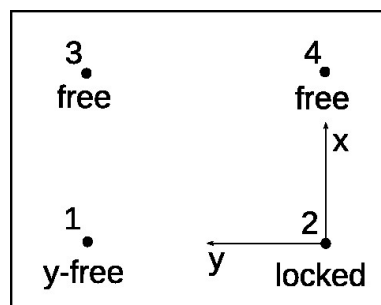
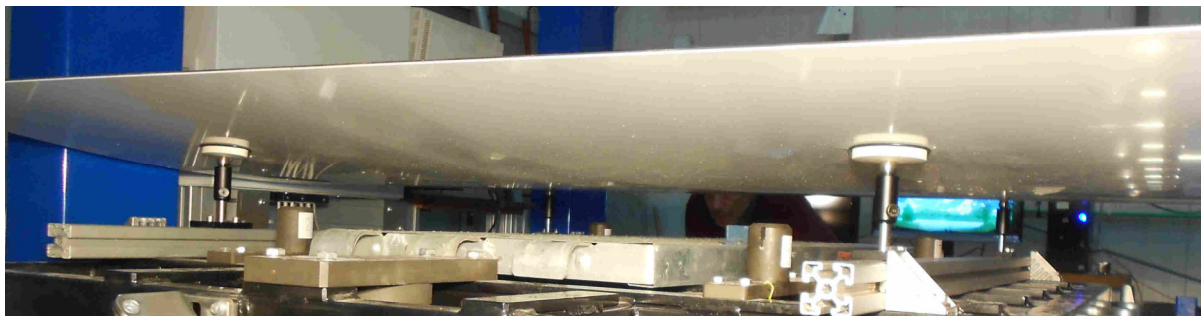


Figure 4.1-1. On the top, view of the supporting system. In the bottom, numbers of the four attaching points and strategy to set their precise positioning in the XY plane of the Lab reference frame.

To be comparable, at the end of the measurements each participant is asked to share results expressed

in the Lab reference frame with the origin in the centre of the metallic ball at the attaching point P2 and Y axis crossing P1, while Z axis is vertical. Because each experimental set-up adopts a different Lab reference frame, the results must be transformed to be comparable.

To discover eventual inconsistency, the results must pass the acceptance check-point consisting of the comparison of the values at the attaching points with the ones expected for the ideal parabola (computed according to Section 3 of [4]). This check can be accomplished by means of the “Tab parameter” of the RRcomparator software.

Such a preliminary check has been very useful to identify some inconsistency generally affecting the first release of the data provided by any participants: this indicates that the transformation of the coordinate system, although it follows well-known laws, is not entirely simple to apply. Anyway, after some initial problems, all participants have been able to deliver valid data-set, which will be shown in the following.

Tables 4.1-1, 4.1-2 and 4.1-3 show the expected z, slopeX and slopeY values of the reflective surface at the 4 attaching points together with mean and standard deviation of the experimental data observed for each participant, except NREL because its evaluation of the absolute 3D shape was not yet provided. For that reason, NREL at this time is not yet included in the comparison of the absolute shape, reported in the next section.

Tab 4.1-1. Mean and standard deviation of z at the inner and outer attaching points for kind of specimens and participants

	Inner		Outer	
	P1&P2 (mm)	P3&P4 (mm)	P1&P2 (mm)	P3&P4 (mm)
Expected	21.09	20.91	20.96	20.88
ENEA	21.45 ± 0.09	20.47 ± 0.10	21.45 ± 0.12	20.40 ± 0.06
F-ISE	21.50 ± 0.41	20.47 ± 0.54	20.77 ± 0.35	21.21 ± 0.25
DLR	21.12 ± 0.01	20.45 ± 0.29	21.01 ± 0.08	20.64 ± 0.26
SANDIA	21.21 ± 0.21	20.32 ± 0.21	20.88 ± 0.13	20.88 ± 0.14

Tab 4.1-2. Mean and standard deviation of slopeX at the inner and outer attaching points for kind of specimens and participants

	Inner	Outer
--	--------------	--------------

	P1&P2	P3&P4	P1&P2	P3&P4
Expected	-0.1358	0.1269	-0.0771	0.0698
ENEA	-0.1345 ± 0.0005	0.1282 ± 0.0014	-0.0801 ± 0.0017	0.0683 ± 0.0009
F-ISE	-0.1340 ± 0.0006	0.1275 ± 0.0017	-0.0782 ± 0.0017	0.0700 ± 0.0009
DLR	-0.1370 ± 0.0042	0.1283 ± 0.0010	-0.0793 ± 0.0021	0.0691 ± 0.0007
SANDIA	-0.1343 ± 0.0010	0.1276 ± 0.0011	-0.0773 ± 0.0017	0.0712 ± 0.0009

Tab 4.1-3. Mean and standard deviation of slopeY at the inner and outer attaching points for kind of specimens and participants

	Inner		Outer	
	P1&P2	P3&P4	P1&P2	P3&P4
Expected	0	0	0	0
ENEA	0.0004 ± 0.0022	0.0009 ± 0.0016	-0.0008 ± 0.0010	-0.0004 ± 0.0008
F-ISE	0.0003 ± 0.0025	0.0010 ± 0.0022	-0.0006 ± 0.0007	-0.0005 ± 0.0005
DLR	-0.0001 ± 0.0019	0.0000 ± 0.0011	-0.0003 ± 0.0010	-0.0006 ± 0.0012
SANDIA	0.0008 ± 0.0011	0.0007 ± 0.0009	0.0002 ± 0.0026	0.0002 ± 0.0026

The values at the attaching points are in satisfactory agreement with the expected values, although the mean value among the experimental data shows a slight systematic deviation; as an example, for inner panels all the experimental mean-z values at P1&P2 are greater than the expected value.

4.2. Comparison with the mean surface

The “true” 3D-surface is unknown and certainly differs from the ideal one. The mean 3D-surface (i.e. the average of the 3D-surfaces provided by all participants) is the best evaluator of the “true” one. Therefore in this section the results obtained by each participant (except NREL) will be compared to the mean 3D-surface.

As discussed in the previous section, the z-value at the four attaching points is satisfactorily close to the expected values for all the participants with a maximum difference less than 1 mm. Nevertheless, to make the comparison more rigorous, we applied a software realignment of the experimental surface to set the z-values at the attaching point at the same values (the ideal ones) for all the participants.

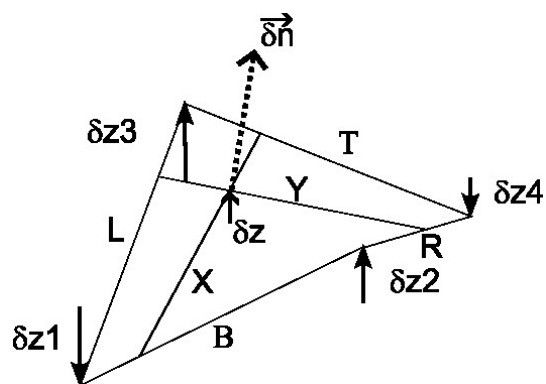


Figure 4.2-1. Sketch of the software realignment of the experimental surface, acting as shift and twist.

More precisely, as shown in Fig 4.2-1, said $\delta z_1, \delta z_2, \delta z_3$ and δz_4 the z-deviation from the ideal value at the attaching points P_1, P_2, P_3, P_4 , let T (top), B (bottom), L (left), and R (right) the four straight lines crossing the couple of points $P_3P_4, P_1P_2, P_1P_3, P_2P_4$, respectively, where $P_j = (x_j, y_j, \delta z_j)$ with $j=1, 2, 3, 4$. Then, the bias of z (δz) and slope ($\delta \vec{n}$) at any point in the XY plane $P=(x, y)$ can be determined by considering the two straight lines X and Y (respectively lying in the planes $y = cte$ and $x = cte$) crossing the straight lines $T\&B$ and $L\&R$, respectively: δz is equal to z of X or Y in P (X and Y intersect in P), while $\delta \vec{n} \approx (m_x, m_y, 1)$, where m_x and m_y are the angular coefficients of the straight lines X and Y , respectively.

Such a software realignment acts like a shift and a twist of the surface which extent depends on the x,y coordinates of the point of application.

Once the data of all participants are loaded and unbiased with the option “SW realignment by devZ_ideal” (i.e. the difference $z - z_{ideal}$ calculated by the software on the basis of z values provided by the participant), the RRcomparator software allows to compare the results obtained by each participant with the mean surface, displaying mean, RMS and Peak-Valley of the difference (see the bottom of the GUI shown in Fig. 3-1); to make more homogeneous the comparison the option “Limited to the common XY area” is ticked.

Tables 4.2-1, 4.2-2 and 4.2.3 summarize the deviations (RMS) respectively for z, slopeX and slopeY, for participants and specimen; the minimum and maximum values are highlighted in *italic* and **bold**, respectively.

Tab 4.2-1. RMS z deviation (mm) from the mean surface

	ENEA	F-ISE	DLR	SANDIA
Inner#60	<u>0.11</u>	0.16	0.16	0.27
Inner#61	<u>0.18</u>	0.23	0.37	0.24
Inner#62	<u>0.10</u>	0.15	0.14	0.27
Outer#93	<u>0.08</u>	0.12	0.15	0.23
Outer#97	<u>0.09</u>	0.11	0.14	0.19
Outer#99	<u>0.07</u>	0.13	0.16	0.21

Tab 4.2-2. RMS slopeX deviation (mrad) from the mean surface

	ENEA	F-ISE	DLR	SANDIA
Inner#60	0.54	0.55	<u>0.35</u>	0.78
Inner#61	1.07	<u>1.05</u>	2.72	1.18
Inner#62	0.58	0.97	<u>0.41</u>	0.89
Outer#93	<u>0.30</u>	0.34	0.38	0.47
Outer#97	0.36	0.32	<u>0.23</u>	0.43
Outer#99	0.28	0.29	<u>0.22</u>	0.54

Tab 4.2-3. RMS slopeY deviation (mrad) from the mean surface

	ENEA	F-ISE	DLR	SANDIA
Inner#60	<u>0.22</u>	0.66	0.51	0.32
Inner#61	<u>0.19</u>	<u>0.19</u>	0.51	0.27
Inner#62	0.27	0.77	0.54	<u>0.26</u>
Outer#93	<u>0.19</u>	0.40	0.33	0.35
Outer#97	<u>0.20</u>	0.42	0.32	0.38
Outer#99	0.27	0.46	0.38	<u>0.26</u>

Except for specimen Inner#61, the RMS-deviation from the mean surface of z and slopes are less than 0.3 mm and 0.8 mrad, respectively, proving a quite good agreement among the participants.

For the sake of brevity, a more exhaustive comparison is reported in the following for just two specimens, Inner#60 and Outer#99, showing for each participant the 2D contour-map of the difference and the graph of the two sections with the planes $y = cte$ crossing the pair of attaching points P₁P₃ and P₂P₄, respectively drawn in red and green.

Tab 4.2-4. Inner#60 – z deviation from the mean surface

	Mean (mm)	RMS (mm)	Peak-Valley (mm)
ENEA	-0.04	<u>0.11</u>	<u>0.67</u>
F-ISE	0.02	0.16	0.88
DLR	-0.08	0.16	0.81
SANDIA	0.10	0.27	1.69

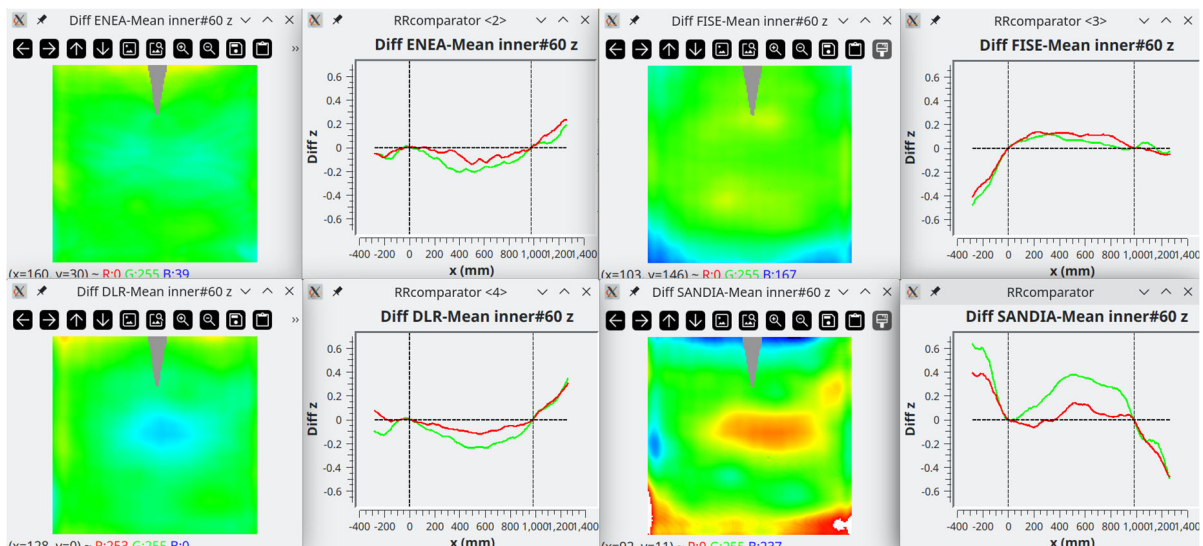


Figure 4.2-2. 2D-contour maps and plots of the section P1-P3 and P2-P4 of z deviation from the mean values for Inner#60.

Tab 4.2-5. Inner#60 – slopeX deviation from the mean surface

	Mean (mrad)	RMS (mrad)	Peak-Valley (mrad)
ENEA	0.15	0.54	4.45
F-ISE	0.21	0.55	5.28
DLR	0.24	<u>0.35</u>	<u>1.68</u>
SANDIA	-0.60	0.78	4.53

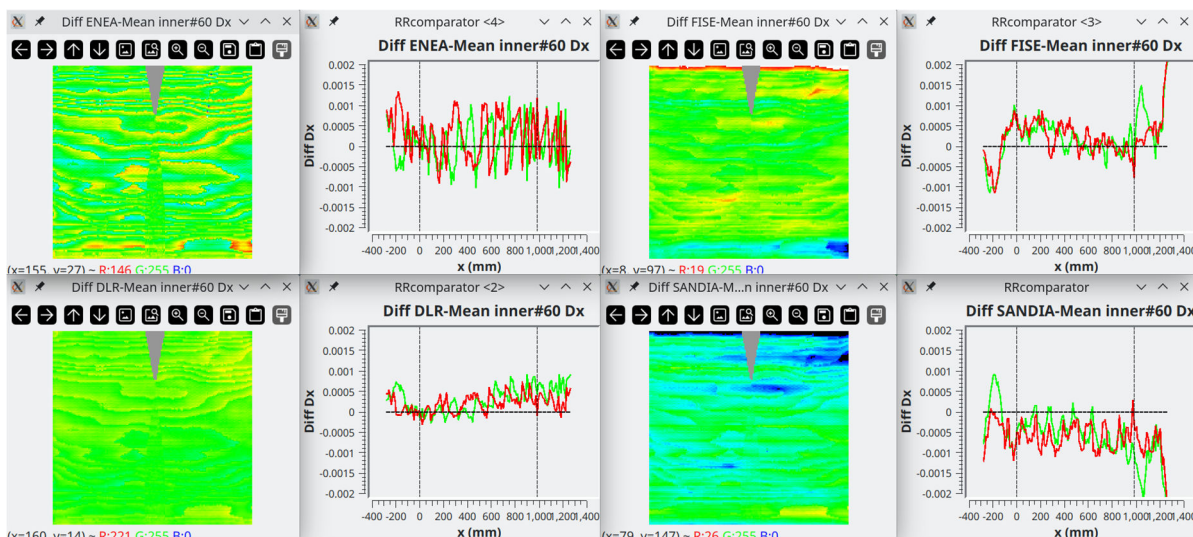


Figure 4.2-3. 2D-contour maps and plots of the section P1-P3 and P2-P4 of slopeX deviation from the mean values for Inner#60.

Tab 4.2-6. Inner#60 – slopeY deviation from the mean surface

	Mean (mrad)	RMS (mrad)	Peak-Valley (mrad)
ENEA	0.10	<u>0.22</u>	<u>2.07</u>
F-ISE	0.08	0.66	4.02
DLR	0.01	0.51	3.32
SANDIA	-0.19	0.32	2.32

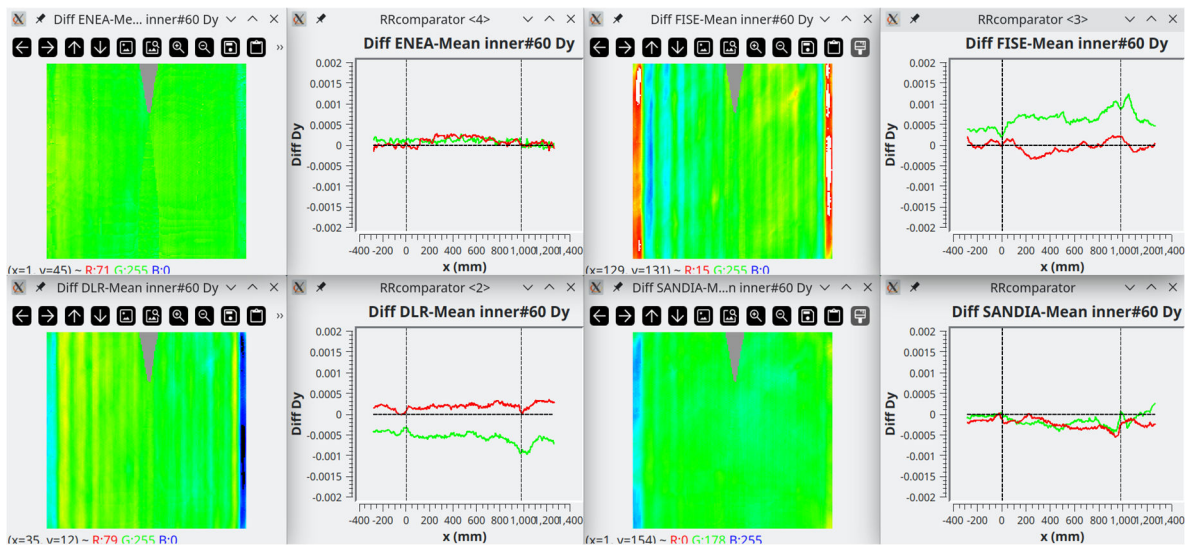
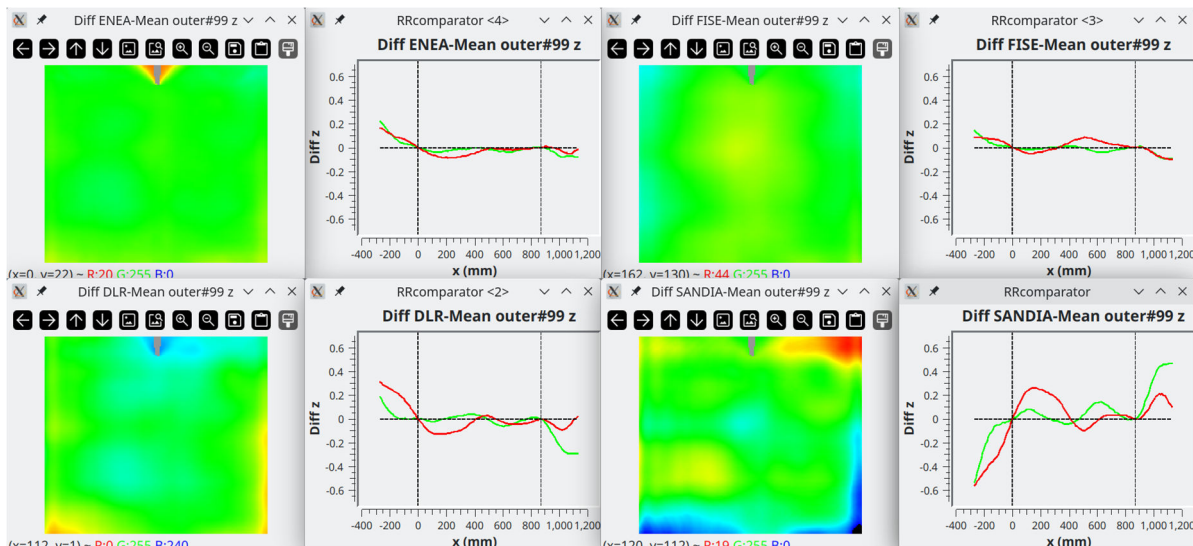


Figure 4.2-4. 2D-contour maps and plots of the section P1-P3 and P2-P4 of slopeY deviation from the mean values for Inner#60.

Tab 4.2-7. Outer#99 – z deviation from the mean surface

	Mean (mm)	RMS (mm)	Peak-Valley (mm)
ENEA	0.02	<u>0.07</u>	0.74
F-ISE	0.03	0.13	<u>0.62</u>
DLR	-0.04	0.16	0.96
SANDIA	-0.01	0.21	1.53

**Figure 4.2-2. 2D-contour maps and plots of the section P1-P3 and P2-P4 of z deviation from the mean values for Outer#99.**

Tab 4.2-8. Outer#99 – slopeX deviation from the mean surface

	Mean (mrad)	RMS (mrad)	Peak-Valley (mrad)
ENEA	-0.14	0.28	2.23
F-ISE	-0.20	0.29	2.09
DLR	-0.13	<u>0.22</u>	<u>1.41</u>
SANDIA	0.47	0.54	1.80

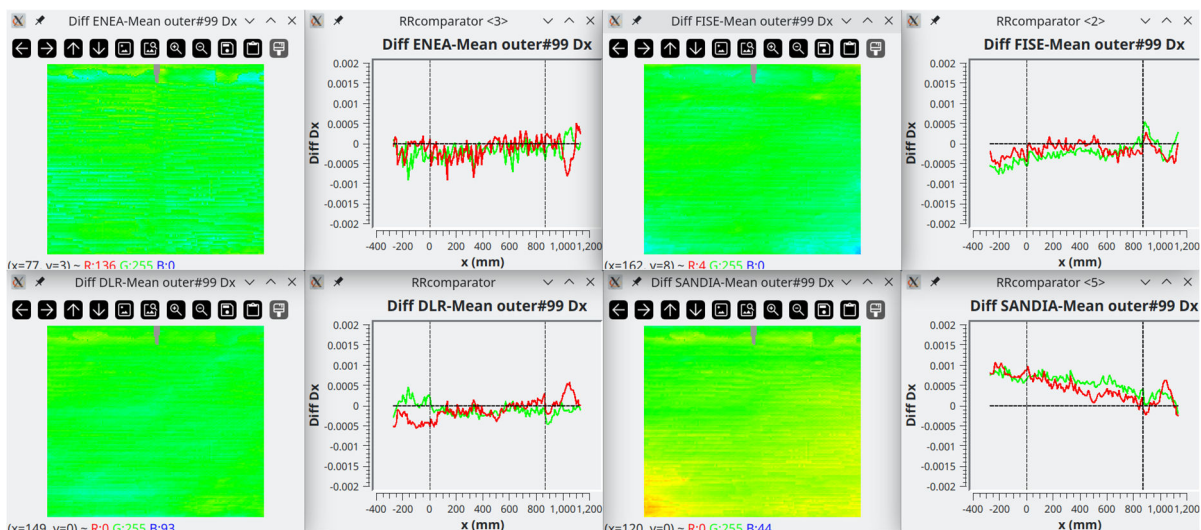
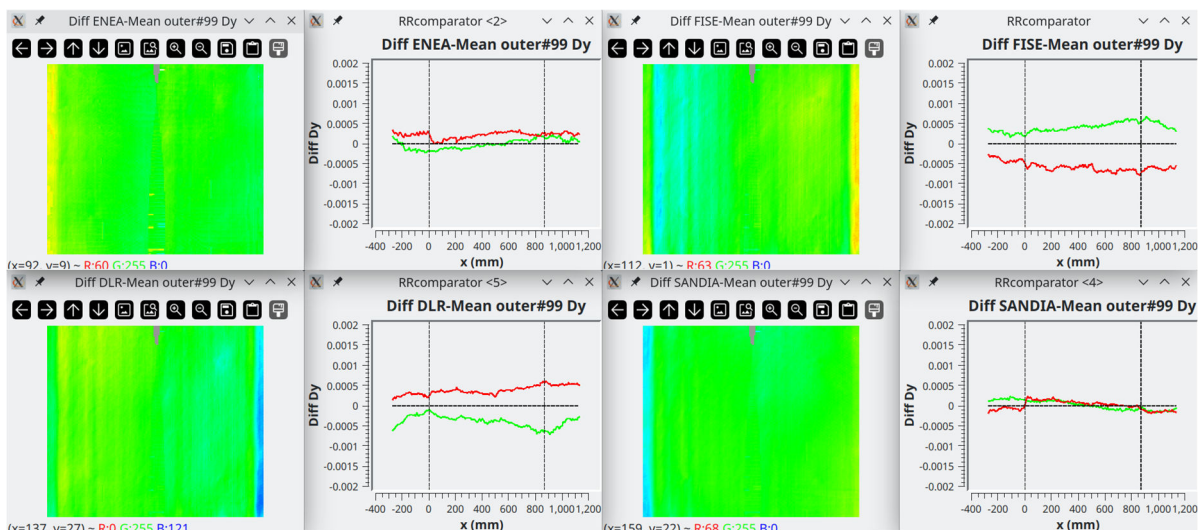


Figure 4.2-3. 2D-contour maps and plots of the section P1-P3 and P2-P4 of slopeX deviation from the mean values for Outer#99.

Tab 4.2-6. Outer#99 – slopeY deviation from the mean surface

	Mean (mrad)	RMS (mrad)	Peak-Valley (mrad)
ENEA	0.07	0.27	2.91
F-ISE	-0.02	0.46	2.40
DLR	-0.02	0.38	2.38
SANDIA	-0.04	<u>0.26</u>	<u>1.90</u>

**Figure 4.2-4. 2D-contour maps and plots of the section P1-P3 and P2-P4 of slopeY deviation from the mean values for Outer#99.**

Considering that to evaluate the performance of PT panels is advisable to have accuracy better than 1 mm and 1 mrad, respectively in z and slope, the results obtained by the various participants are in very good agreement.

5. Comparison of the deviation from the ideal parabola

The comparison of the 3D-shape, discussed in the previous section, is important to study the reliability of the adopted instruments to measure the shape of reflective panels in absolute terms.

On the other hand, in practice these set-ups are used to evaluate the compliance of the panels with the ideal parabola, by giving the RMS deviation of z and slopes; this section aims to compare these predictions.

At the time of drafting the present report, NREL provided limited data for Inner#60, Inner#62, Outer#93 and Outer#97, without z and slopeX values; in the near future the remaining data will be provided.

Initially, the statistical analysis of the deviation from the ideal parabola as evaluated by each participant is accomplished by loading in RRcomparator the data-set as it is, without applying any software re-alignment.

The tables 5-1, 5-2 and 5-3 are filled with the values displayed in the “Tab statistics” once one parameter among devZ, devSlopeX and devSlopeY is selected. Once again, the minimum and maximum values are highlighted in *italic* and **bold**, respectively.

Tab 5-1. RMS z deviation (mm) from the ideal parabola

	ENEA	F-ISE	DLR	SANDIA	NREL
Inner#60	0.47	0.64	0.50	<u>0.39</u>	
Inner#61	<u>0.50</u>	0.72	0.52	0.52	
Inner#62	0.41	0.53	0.44	<u>0.29</u>	
Outer#93	0.72	0.36	0.55	<u>0.22</u>	
Outer#97	0.68	0.39	0.50	<u>0.31</u>	
Outer#99	0.80	0.41	0.55	<u>0.19</u>	

Tab 5-2. RMS slopeX deviation (mrad) from the ideal parabola

	ENEA	F-ISE	DLR	SANDIA	NREL
Inner#60	2.63	2.98	2.84	2.79	<u>1.94</u>
Inner#61	<u>2.63</u>	3.07	4.04	3.08	
Inner#62	2.17	2.33	2.52	2.39	<u>1.79</u>
Outer#93	2.31	1.57	1.71	1.49	<u>1.30</u>
Outer#97	2.22	1.55	1.67	1.52	<u>1.24</u>
Outer#99	2.50	1.53	1.81	<u>1.50</u>	

Tab 5-3. RMS slopeY deviation (mrad) from the ideal parabola

	ENEA	F-ISE	DLR	SANDIA	NREL
Inner#60	2.76	<u>2.21</u>	2.88	3.00	2.26
Inner#61	2.77	<u>2.17</u>	2.99	3.01	
Inner#62	2.68	2.20	2.87	2.92	<u>2.18</u>
Outer#93	2.14	<u>1.73</u>	2.73	2.00	2.19
Outer#97	1.99	1.63	2.51	2.06	<u>1.29</u>
Outer#99	2.13	<u>1.61</u>	2.67	1.97	

The maximum difference among z-deviation, slopeX-deviation and slopeY-deviation is 0.6 mm, 1.4 mrad, and 1.2 mrad, respectively. Although these results are not discouraging, the agreement is a bit worse compared to the case of the absolute shape (see section 4).

To better understand the reason of this partial disagreement, the analysis of mean value and standard deviation of RMS values is very useful. In particular, the second column of tables 5-4, 5-5, and 5-6 reports mean value and standard deviation of the RMS deviations provided by the participants; third and fourth columns shown the effect of limiting the statistics to the common XY region without and with the “SW realignment by devZ_exp” (i.e. the difference $z - z_{ideal}$ directly provided by the participant, listed in the 6th column of the result file), respectively. As matter of fact the difference

among the scanned areas from the several instruments can bring to apparent disagreement; another source of apparent disagreement is the imperfect positioning of the specimens on the four attaching points. Tables 5-4, 5-5, and 5-6 proves that the software realignment is the most important action to do for increasing the agreement among the participants.

Tab 5-4. Mean and standard deviation of the z-deviations from the ideal parabola as it is, limited to the common XY area, and applying the software realignment

	As it is (mm)	XY common (mm)	XY common and SW realignment (mm)
Inner#60	0.50 ± 0.09	0.47 ± 0.10	0.46 ± 0.08
Inner#61	0.56 ± 0.10	0.54 ± 0.10	0.48 ± 0.08
Inner#62	0.42 ± 0.10	0.39 ± 0.09	0.34 ± 0.06
Outer#93	0.47 ± 0.19	0.45 ± 0.18	0.34 ± 0.08
Outer#97	0.47 ± 0.14	0.45 ± 0.13	0.32 ± 0.08
Outer#99	0.49 ± 0.22	0.46 ± 0.20	0.30 ± 0.09

Tab 5-5. Mean and standard deviation of the slopeX-deviations from the ideal parabola as it is, limited to the common XY area, and applying the software realignment

	As it is (mrad)	XY common (mrad)	XY common and SW realignment (mrad)
Inner#60	2.64 ± 0.36	2.40 ± 0.37	2.45 ± 0.42
Inner#61	3.21 ± 0.51	2.99 ± 0.51	3.04 ± 0.50
Inner#62	2.24 ± 0.25	2.06 ± 0.22	2.04 ± 0.19
Outer#93	1.68 ± 0.34	1.63 ± 0.35	1.50 ± 0.16
Outer#97	1.64 ± 0.32	1.60 ± 0.34	1.44 ± 0.16
Outer#99	1.83 ± 0.40	1.80 ± 0.41	1.57 ± 0.08

Tab 5-6. Mean and standard deviation of the slopeY-deviations from the ideal parabola as it is, limited to the common XY area, and applying the software realignment

	As it is (mrad)	XY common (mrad)	XY common and SW realignment (mrad)
Inner#60	2.62 ± 0.33	1.60 ± 0.07	1.59 ± 0.05
Inner#61	2.73 ± 0.34	2.30 ± 0.10	2.28 ± 0.09
Inner#62	2.57 ± 0.32	1.60 ± 0.14	1.58 ± 0.13
Outer#93	2.16 ± 0.33	1.85 ± 0.21	1.82 ± 0.20
Outer#97	1.90 ± 0.41	1.61 ± 0.26	1.58 ± 0.26
Outer#99	2.10 ± 0.38	1.86 ± 0.24	1.83 ± 0.26

For the sake of brevity, a more exhaustive comparison is reported in the following for just two specimens, Inner#60 and Outer#93, showing for each participant the 2D contour-map of the difference and the graph of the two sections with the planes $y = cte$ crossing the pair of attaching points P₁P₃ and P₂P₄, respectively drawn in red and green.

The comparison concerns the results obtained considering the common XY region with the "SW realignment by devZ_exp" option.

NREL is included only in the comparison of the slope deviation.

Tab 5-7. Inner#60 – z deviation from the ideal parabola

	Mean (mm)	RMS (mm)	Peak-Valley (mm)
ENEA	-0.05	0.45	3.07
F-ISE	0.01	0.59	3.33
DLR	-0.09	0.44	2.82
SANDIA	0.09	<u>0.36</u>	<u>1.82</u>
NREL	NA	NA	NA

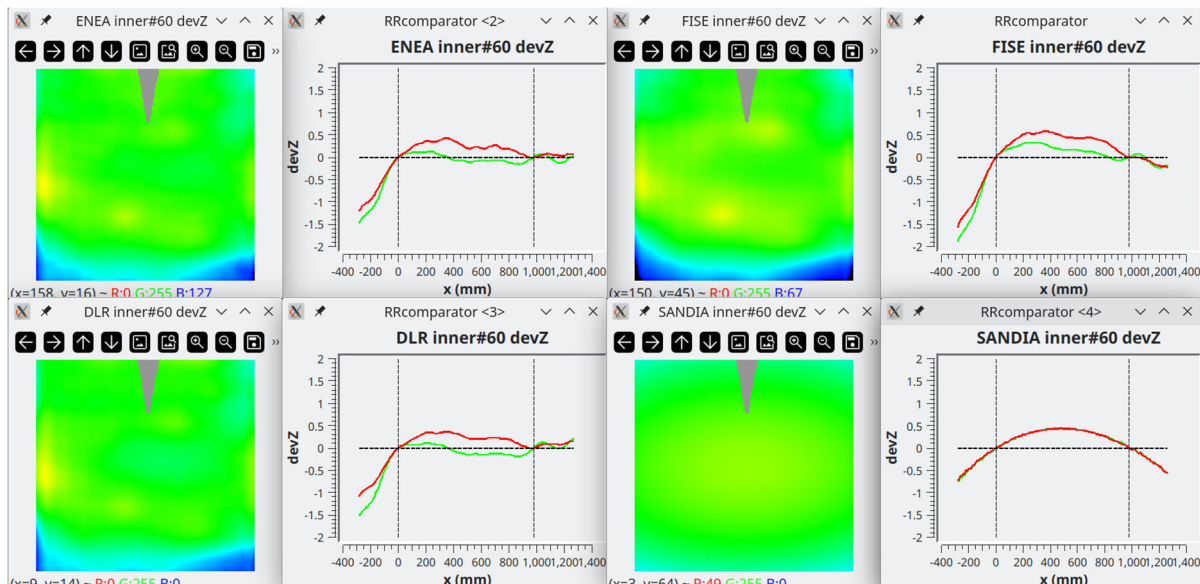
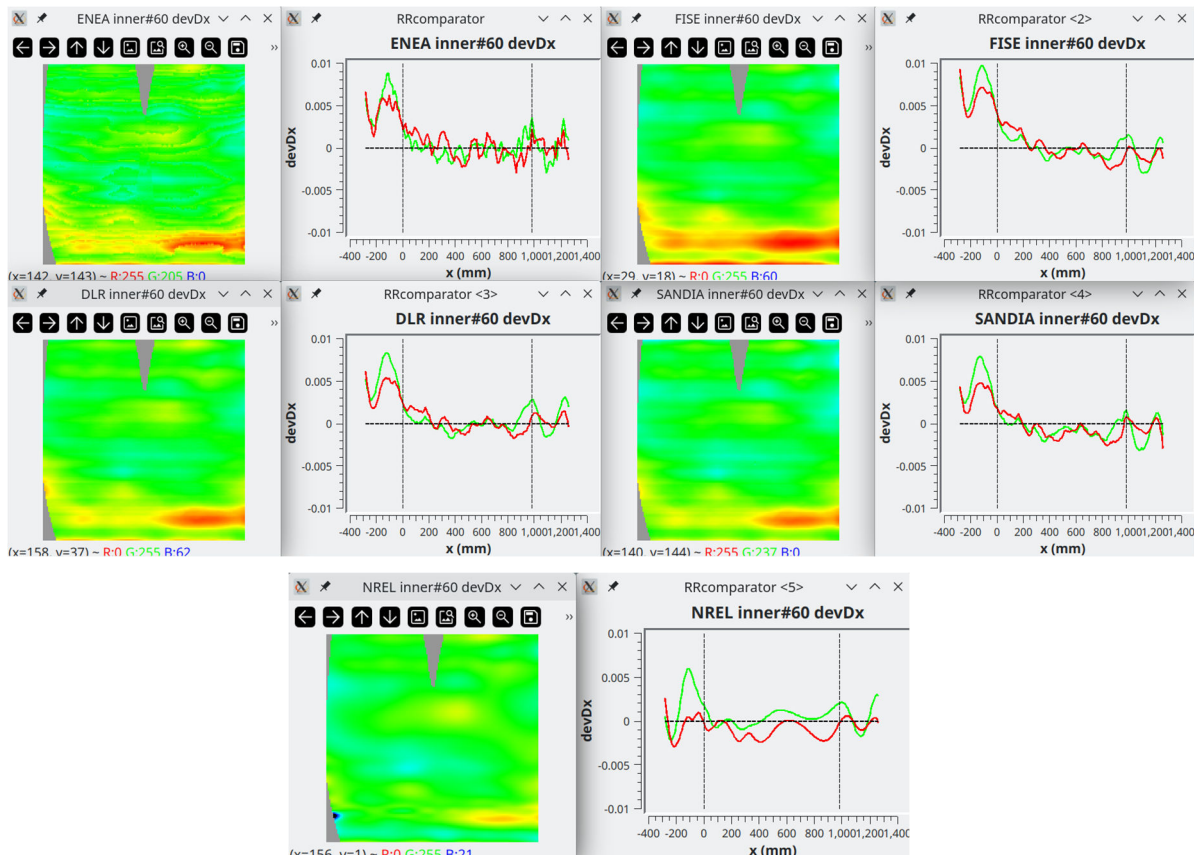


Figure 5-1. 2D-contour maps and plots of the section P1-P3 and P2-P4 of z deviation from the ideal parabola for Inner#60.

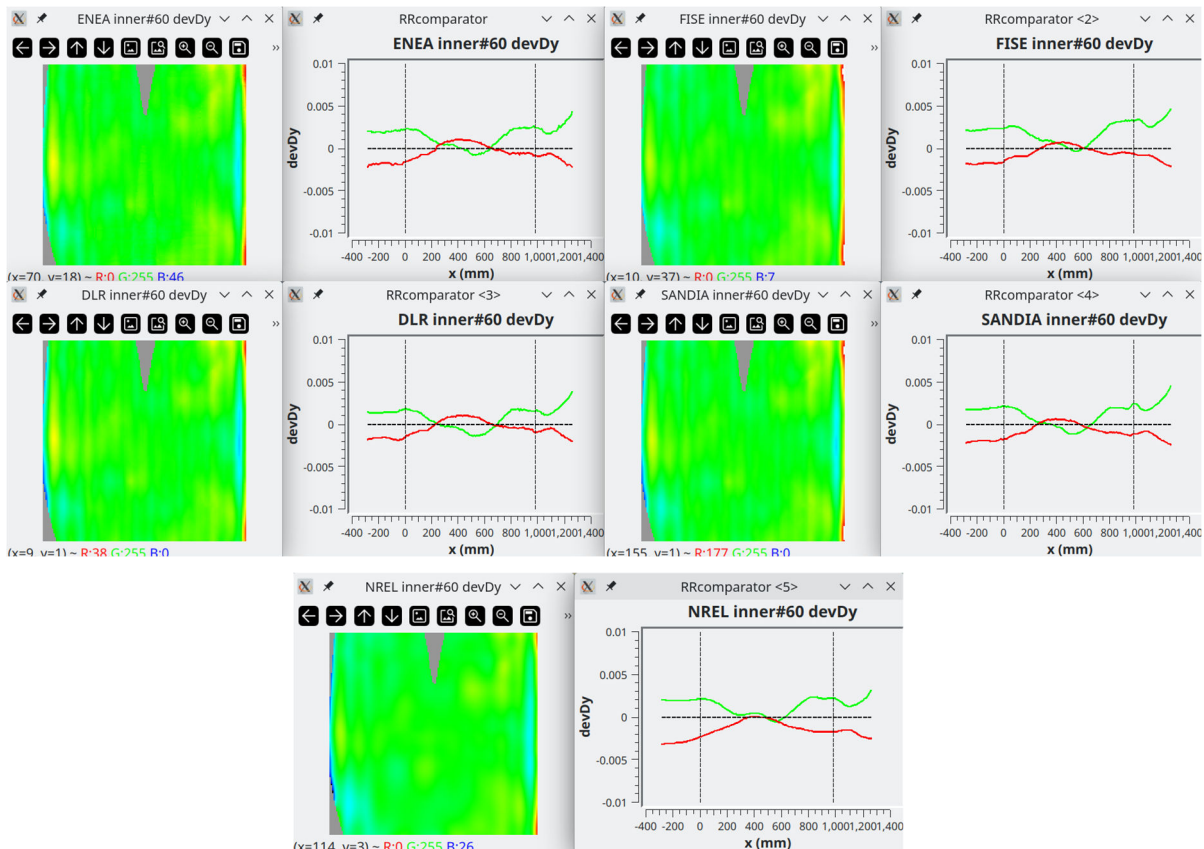
Tab 5-8. Inner#60 – slopeX deviation from the ideal parabola

	Mean (mrad)	RMS (mrad)	Peak-Valley (mrad)
ENEA	0.82	2.55	14.74
F-ISE	1.00	3.12	15.13
DLR	0.89	<u>2.41</u>	<u>12.18</u>
SANDIA	0.10	2.37	13.80
NREL	-0.10	1.81	<u>21.35</u>

**Figure 5-2. 2D-contour maps and plots of the section P1-P3 and P2-P4 of slopeX deviation from the ideal parabola for Inner#60.**

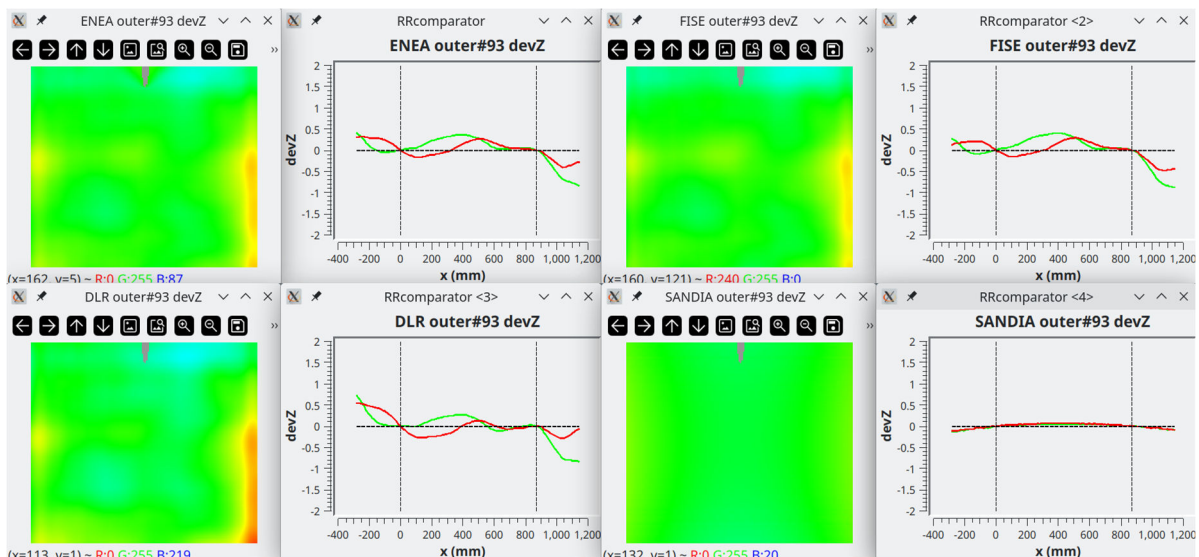
Tab 5-9. Inner#60 – slopeY deviation from the ideal parabola

	Mean (mrad)	RMS (mrad)	Peak-Valley (mrad)
ENEA	0.24	1.55	<u>17.59</u>
F-ISE	0.17	1.68	18.27
DLR	0.18	<u>1.54</u>	18.49
SANDIA	-0.02	1.61	19.67
NREL	-0.34	1.57	19.26


Figure 5-3. 2D-contour maps and plots of the section P1-P3 and P2-P4 of slopeY deviation from the ideal parabola for Inner#60.

Tab 5-10. Outer#93 – z deviation from the ideal parabola

	Mean (mm)	RMS (mm)	Peak-Valley (mm)
ENEA	0.07	0.37	2.08
F-ISE	0.06	0.36	2.02
DLR	0.00	0.44	2.69
SANDIA	-0.02	0.22	0.92
NREL	NA	NA	NA


Figure 5-4. 2D-contour maps and plots of the section P1-P3 and P2-P4 of z deviation from the ideal parabola for Outer#93.

Tab 5-10. Outer#93 – slopeX deviation from the ideal parabola

	Mean (mrad)	RMS (mrad)	Peak-Valley (mrad)
ENEA	-0.58	1.63	9.34
F-ISE	-0.53	1.65	9.57
DLR	-0.62	1.58	<u>8.34</u>
SANDIA	-0.01	1.43	8.13
NREL	-0.02	<u>1.21</u>	<u>7.51</u>

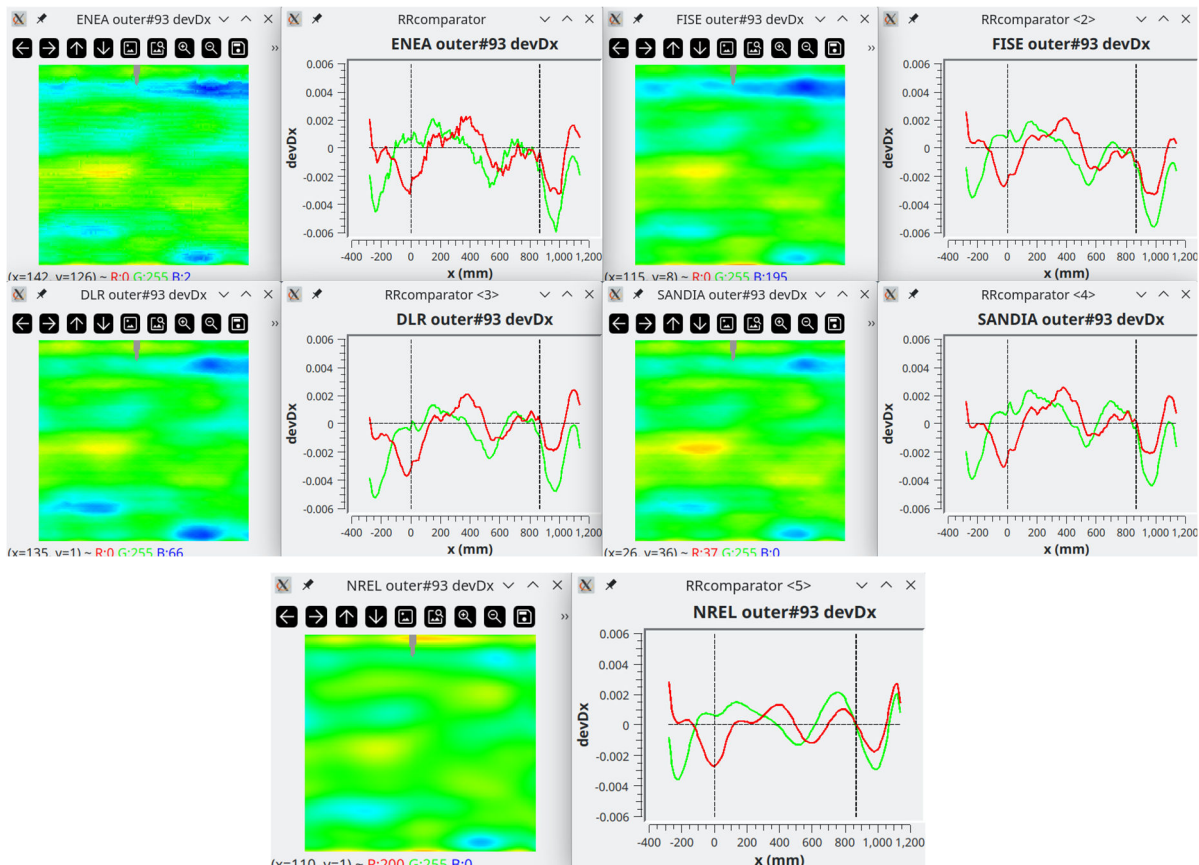


Figure 5-5. 2D-contour maps and plots of the section P1-P3 and P2-P4 of slopeX deviation from the ideal parabola for Outer#93.



GA No: 823802

31.01.2024

Tab 5-11. Outer#93 – slopeY deviation from the ideal parabola

	Mean (mrad)	RMS (mrad)	Peak-Valley (mrad)
ENEA	-0.28	1.78	13.17
F-ISE	-0.28	1.61	<u>13.02</u>
DLR	-0.42	2.18	15.72
SANDIA	-0.11	<u>1.68</u>	15.57
NREL	-0.10	1.87	19.14

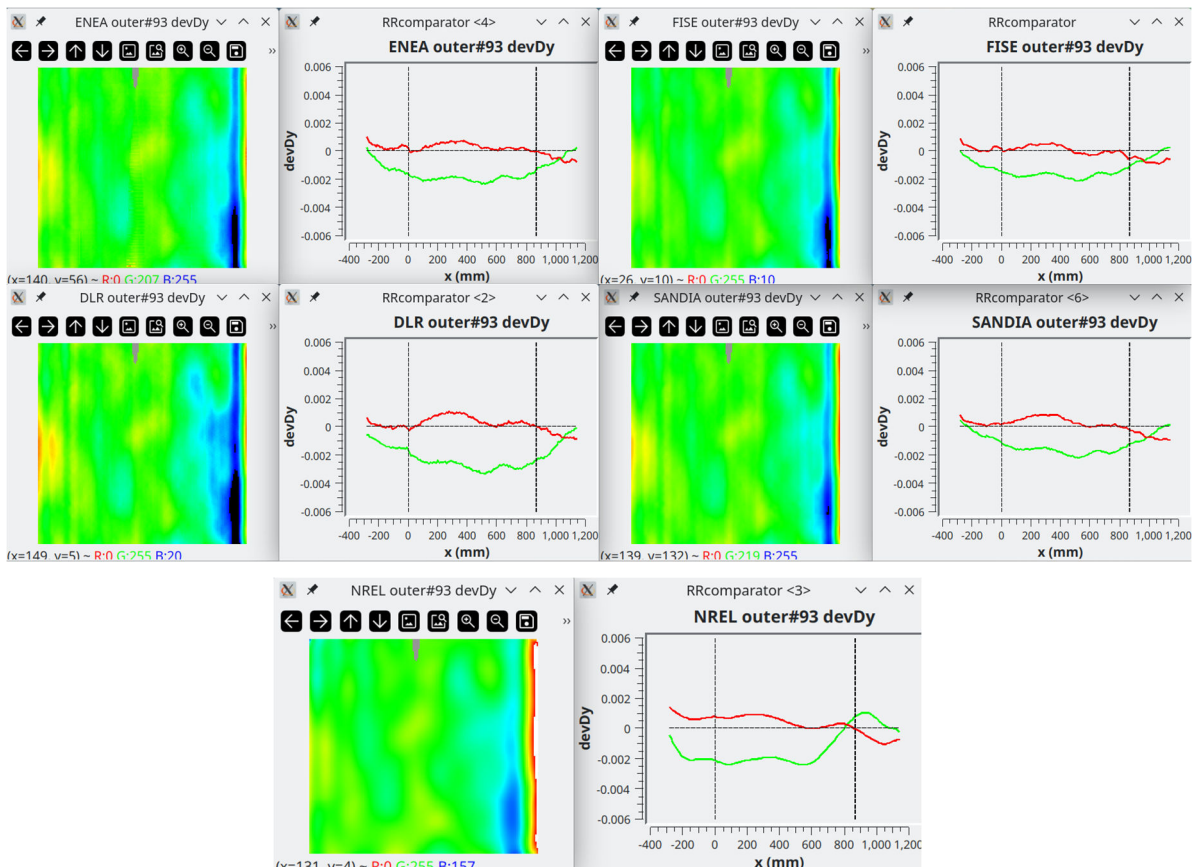


Figure 5-6. 2D-contour maps and plots of the section P1-P3 and P2-P4 of slopeY deviation from the ideal parabola for Outer#99.

In general, for a given specimen, the 2D-contour maps of the same parameter are quite similar one to each other, indicating good agreement among the participants.

Considering the z-deviation, it is evident that SANDIA uses to approximate the z-profile with a parabolic function; that brings to over-smooth the surface and consequently the RMS deviation is under-evaluated.

Because NREL has not yet provided z-deviation data, actually it can not benefit of the software realignment.

6. Conclusions

Since the beginning, the 3D-shape RR has been organized paying great attention to the effect of the specimen placing in the laboratory set-up: being not perfectly rigid, the shape of any PT reflective panel is influenced on how the specimen is supported. In order to overcome that problem ENEA outlined a method [4] to make highly reproducible the specimen placing; although the observed residual z-deviations on the four attaching points were less than 1 mm, in the end that still reduces the agreement among the results got by the participants. Such an effect was successfully reduced by including in RRcomparator software a realignment procedure of the 3D profile on the four attaching points; the agreement among the results of both absolute shape and deviation from the ideal parabola benefited of that realignment: the standard deviation is less than 0.1 mm, 0.5 mrad and 0.3 mrad for z, slopeX and slopeY deviation from the ideal parabola, respectively.

The importance of the supporting system is one of the most important lesson learned with the RR: in the practical case the panel should be firmly lock to the four attaching points, provided that position and tilting of the four mounting brackets have been accurately set accordingly to the manufacturer design.

The beneficial effect of the software realignment is the second important learned lesson. Of course to be applied, the data processing must include the evaluation of the absolute 3D-shape.

Both these lessons should be transferred in the next guidelines on the topic.

7. References

- [1] M. Montecchi, G. Cara, A. Benedetti, "VISproPT: a high precision instrument for 3D shape analysis of parabolic trough panels", Open Research Europe,
<https://doi.org/10.12688/openreseurope.15967.2>
- [2] <https://github.com/mmonty1960/VISproPT>
- [3] <https://www.solarpaces.org/solarpaces-tasks/task-iii-solar-technology-and-advanced-applications/>
- [4] M. Montecchi, G. Cara, A. Benedetti, "Procedure for placing PT-panels in SFERA-III WP10 Task3 3D shape measurement round-robin", <https://github.com/mmonty1960/RRcomparator>
- [5] Montecchi M: Italian Patent. RM2008A000151, 2008
- [6] M. Montecchi, G. Cara, A. Benedetti, "VISproLF: Self-Calibrating Instrument for Measuring 3D Shape of Linear Fresnel Facets", Rev. Sci. Instrum. 91, 083109 (2020); doi: 10.1063/5.0013116
- [7] MARPOSS Italia, <https://www.marposs.com/eng/>
- [8] T. März, C. Prahl, S. Ulmer, S. Wilbert, C. Wilbert: Validation of two Optical Measurement Methods for the Qualification of the Shape Accuracy of Mirror Panels for Concentrating Solar Systems, Proceedings of the SolarPACES 2010 Conference in Perpignan, France, September 21 - 24, 2010
- [9] S. Ulmer, T. März, C. Prahl, W. Reinalter, B. Belhomme: Automated High Resolution Measurement of Heliostat Slope Errors. Proceedings of the SolarPACES conference, 15-18 September 2009, Berlin, Germany
- [10] Lüpfert, Eckhard und Ulmer, Steffen, Solar Trough mirror shape specifications, SolarPACES, Berlin, Deutschland, 2009
- [11] S. Ulmer, P. Heller, W. Reinalter: Slope Measurements of Parabolic Dish Concentrators Using Color Codified Targets. Journal of Solar Energy Engineering, Volume 130, Issue 1, 011015, February 2008

- [12] S. Ulmer, K. Pottler, E. Lüpfert, M. Röger: Measurement Techniques for the Optical Quality Assessment of Parabolic Trough Collector Fields in Commercial Solar Power Plants. Proceedings of ES2007, Energy Sustainability 2007, June 27-30, 2007, Long Beach, California, USA
- [13] C. Andraka, et al. Rapid Reflective Facet Characterization Using Fringe Reflection Techniques. *Journal of Solar Energy Engineering* **136**, February 2014
- [14] R. C. Brost, B. J. Smith, F. M. Brimigion, and A. T. Evans. Extending Deflectometry Metrology Capability for CSP. Presented in the *ES 2023 17th International Conference on Energy Sustainability*, Washington, DC, July 2023
- [15] Rrcomparator software is downloadable from <https://github.com/mmonty1960/RRcomparator>